Data-Driven material identification in heterogeneous viscoelastic media

Hossein Salahshoor, Michael Ortiz, Laurent Stainier

DATA-DRIVEN MATERIAL IDENTIFICATION IN HETEROGENEOUS VISCOELASTIC MEDIA

HOSSEIN SALAHSHOOR[1,2], MICHAEL ORTIZ[3,4], LAURENT STAINIER[5]

Abstract. Full-field material characterization techniques are increasingly improving and new techniques are emerging, providing us altogether with unprecedented access to kinematic measurements. Extracting material properties from data has been a long quest, with the challenge lying at extricating homogeneity in inference and enabling extraction of spatially-varying mechanical properties. We propose a data-driven approach here that enables identifying heterogeneous properties of linear media, either elastic or viscoelastic. We reformulate the identification problem to that of identifying a set in a phase space of possible stresses and strains and employ a hyper-plane data clustering approach algorithm to infer the pointwise material set.

1. Introduction

Material identification from empirical data may be understood as an inverse problem (see, e. g., the pioneering work of Bui [1]). Recent advances in experimental techniques, including the ability to perform spatially and time-resolved measurements [2, 3], high-throughput experiments [4, 5] and elastography techniques for the characterization of biological tissue [6, 7], have provided renewed impetus to the subject. In addition, neural networks and machine learning have supplied a new and efficient means of representing material laws and fitting them by regression to big data sets, prompting an extensive reevaluation of the field. These advances notwithstanding, many questions remain open regarding identifiability, convergence with respect to data and others (see, e. g., [8] for a discussion of mathematical issues).

For the most part, the classical work is concerned mainly with the identification of parameters in a given class of models, in contrast to the more challenging problem of identifying the functional form of the model itself (see, e. g., [9] and references therein). In this setting, material characterization is often viewed as the problem of finding underlying manifolds that represent data [10], and has been addressed through a number of approaches from regression [11], to PDE-constrained optimization and adjoint methods [12, 13, 14], to deep learning [15, 16] and data-driven-identification (DDI) [17]. A review on model updating methods is proposed in [18]. A model-discovery approach based on sparse regression has recently been proposed

by [19], for hyperelasticity. The (model-free) data-driven identification approach has been applied to hyperelasticity [20, 21], elastoplasticity [22, 23], or viscoelasticity [24].

Identifying *heterogeneous* material response from experimental measurements constitutes a further long-standing challenge in mechanics. Recent developments in microscopy that grant access to full-field measurements of the mechanical response of materials [25, 26, 27] have rekindled the need for robust identification approaches and high-resolution inference methods capable of extracting spatially-resolved material properties.

In this work, we develop a data-driven procedure that supplies spatially-resolved elastic and viscoelastic properties of a heterogeneous solid. In the latter case, we work in the frequency domain at fixed frequency, which reduces the identification problem to resolving the spatial distribution of complex moduli over the solid. We combine of a model-free approach (DDI), which identifies a balanced stress field correlated to the measured strains, to a model-based parameter identification approach which identifies moduli and their distribution. This latter approach relies on previous work by Cherkaev and Gibiansky [28], who introduced mixed energy functions that recast the viscoelastic constitutive relations in variational form. In addition, the mixed energy functions are convex and therefore set forth a minimum principle for the solutions. Exploiting this convexity, an inverse procedure can then be built using the duality gap [29, 30, 31, 32, 33], which satisfies Fenchel's inequality [34], as a natural cost function for purposes of identification. We perform the minimization of the cost with respect to the parameters by means of *k-planes clustering* [35]. This algorithm alternates between assigning clusters and using principal component analysis to find normal vectors to each cluster and is robust in the presence of noise [36]. DDI results provide data for initializing this alternate minimization.

2. Heterogeneous Material identification

2.1. **Boundary-value problems in mechanics.** The solutions to boundary-value problems of mechanics consist of displacement, strain and stress fields, respectively denoted by $\boldsymbol{u}$, $\boldsymbol{\varepsilon}$ and $\boldsymbol{\sigma}$ in the following. We restrict ourselves to linearized kinematics and quasi-static loading. These fields must verify the field equations of compatibility, equilibrium and the constitutive relations.

For the sake of conciseness, we directly place ourselves in a discrete context, where compatibility can be simply written as

$$\boldsymbol{\varepsilon}_e = \mathbf{B}_e \mathbf{u} \quad e \in \{1, 2, \cdots, M\}. \tag{1}$$

with the discrete gradient operator $\mathbf{B}_e$ allowing to compute strains at material point e from the array of displacement degrees of freedom (e.g. nodal values in finite elements). Quasistatic balance equations can then be written

as

$$\sum_{e=1}^{M} w_e \mathbf{B}_e^T \boldsymbol{\sigma}_e = \mathbf{f}, \tag{2}$$

where w_e denotes the weight associated to material point e and $\mathbf{f}$ is an array of applied forces, conjugate to $\mathbf{u}$.

In order to close the problem, additional equations should be provided, linking strain and stress tensors. The traditional approach consists in writing constitutive relations of the form $\boldsymbol{\sigma} = \hat{\boldsymbol{\sigma}}(\boldsymbol{\varepsilon}; p)$ where $\hat{\boldsymbol{\sigma}}(\bullet; p)$ is a postulated function parameterized by p. Introducing these relations in the equilibrium equation yields

$$\sum_{e=1}^{M} w_e \mathbf{B}_e^T \hat{\boldsymbol{\sigma}}(\mathbf{B}_e \mathbf{u}) = \mathbf{f}, \tag{3}$$

which provides a set of (potentially nonlinear) equations for $\mathbf{u}$. Note that kinematic (Dirichlet) boundary conditions typically constrain some components of $\mathbf{u}$ to take prescribed values.

2.2. **Constitutive gap approach.** As discussed in more detail below (section 3), an alternative way to represent the constitutive response is through the so-called constitutive gap, or Fenchel, function $G(\boldsymbol{\varepsilon}, \boldsymbol{\sigma}; p)$, with p representing the set of parameters. This function is required to be convex and satisfy

$$G(\boldsymbol{\varepsilon}, \hat{\boldsymbol{\sigma}}(\boldsymbol{\varepsilon}); p) = 0, \tag{4a}$$

$$G(\boldsymbol{\varepsilon}, \boldsymbol{\sigma}; p) > 0, \quad \text{if } \boldsymbol{\sigma} \neq \hat{\boldsymbol{\sigma}}(\boldsymbol{\varepsilon}), \tag{4b}$$

or

$$\hat{\boldsymbol{\sigma}}(\boldsymbol{\varepsilon}; p) = \arg\min_{\boldsymbol{\sigma}} G(\boldsymbol{\varepsilon}, \boldsymbol{\sigma}; p), \tag{5}$$

providing an implicit constitutive relation. A classical example concerns a convex strain-energy density $W(\boldsymbol{\varepsilon}; p)$, with dual complementary energy $W^*(\boldsymbol{\sigma}; p)$. Then, the corresponding Fenchel function

$$G(\boldsymbol{\varepsilon}, \boldsymbol{\sigma}; p) = W(\boldsymbol{\varepsilon}; p) + W^*(\boldsymbol{\sigma}; p) - \boldsymbol{\sigma} \cdot \boldsymbol{\varepsilon}, \tag{6}$$

is convex and defines a constitutive gap function in the sense of (4) (see [34, Thm. 31.1]). The problem of elasticity can then be reformulated as

$$\min_{\mathbf{u}, \{\boldsymbol{\sigma}_e\} \text{ adm.}} \sum_{e=1}^{M} w_e G(\mathbf{B}_e \mathbf{u}, \boldsymbol{\sigma}_e; p), \tag{7}$$

where admissible displacements and stresses are those verifying kinematic boundary conditions and equilibrium (2).

2.3. **Material identification.** Consider the case where measured displacement fields $\mathbf{u}_{\text{exp}}$ are available, together with the loading $\mathbf{f}$. The following inverse problem can then be formulated

$$(\{\boldsymbol{\sigma}_e\}, p) = \arg \min_{\{\boldsymbol{\sigma}_e\} \text{ adm.}, p} \sum_{e=1}^{M} w_e G(\mathbf{B}_e \mathbf{u}_{\text{exp}}, \boldsymbol{\sigma}_e; p), \tag{8}$$

seeking to find a balanced stress field and a set of constitutive parameters which minimize the constitutive gap. Note that heterogeneous materials can be considered, for example by considering that p groups different parameters subsets: $p = \{p_i, i = 1, \dots, N\}$. The minimization then becomes combinatorial

$$(\{\boldsymbol{\sigma}_e\}, p) = \arg \min_{\{\boldsymbol{\sigma}_e\} \text{ adm.}, p, \{i_e\}} \sum_{e=1}^{M} w_e G(\mathbf{B}_e \mathbf{u}_{\text{exp}}, \boldsymbol{\sigma}_e; p_{i_e}), \tag{9}$$

where we assume that the gap function G can represent the different materials. Alternatively, it is possible to consider a number of separate gap functions G_i.

Depending on the exact expression of the chosen constitutive gap function, this minimization problem may be more or less difficult to solve numerically. Alternated minimization approaches can typically be used, but we postpone that discussion and first illustrate different types of constitutive gap functions.

3. Model based constitutive gap

3.1. **Linear elasticity.** Linear elastic materials are characterized by a stiffness tensor $\mathbb{C}$:

$$\boldsymbol{\sigma} = \mathbb{C} : \boldsymbol{\varepsilon}, \tag{10}$$

where $\boldsymbol{\varepsilon}$ and $\boldsymbol{\sigma}$ are the strain and stress second-order tensors, respectively.

Constitutive relation (10) can alternatively be represented by the stored energy potential $W(\boldsymbol{\varepsilon})$:

$$W(\boldsymbol{\varepsilon}) = \frac{1}{2} \boldsymbol{\varepsilon} : \mathbb{C} : \boldsymbol{\varepsilon}, \tag{11}$$

such that

$$\boldsymbol{\sigma} = \frac{\partial W}{\partial \boldsymbol{\varepsilon}} (\boldsymbol{\varepsilon}) \,. \tag{12}$$

The constitutive relation can also be represented through the dual potential $W^*(\boldsymbol{\sigma})$:

$$W^*(\boldsymbol{\sigma}) = \frac{1}{2} \boldsymbol{\sigma} : \mathbb{C}^{-1} : \boldsymbol{\sigma}, \tag{13}$$

such that

$$\boldsymbol{\varepsilon} = \frac{\partial W^*}{\partial \boldsymbol{\sigma}} (\boldsymbol{\sigma}) \,. \tag{14}$$

One can then define the function

$$G(\boldsymbol{\varepsilon}, \boldsymbol{\sigma}) = W(\boldsymbol{\varepsilon}) + W^*(\boldsymbol{\sigma}) - \boldsymbol{\sigma} : \boldsymbol{\varepsilon}, \tag{15}$$

which, when $\mathbb{C}$ is positive-definite, has the following properties:

$$G(\boldsymbol{\varepsilon}, \boldsymbol{\sigma}) \geq 0 \quad \text{and} \quad G(\boldsymbol{\varepsilon}, \boldsymbol{\sigma}) = 0 \iff \boldsymbol{\sigma} = \mathbb{C} : \boldsymbol{\varepsilon}\,. \tag{16}$$

The function $G(\boldsymbol{\varepsilon}, \boldsymbol{\sigma})$ then defines a constitutive gap measuring the discrepancy of an arbitrary pair $(\boldsymbol{\varepsilon}, \boldsymbol{\sigma})$ with respect to the constitutive relation (10). The parameters are then the elastic moduli composing $\mathbb{C}$ at all material points.

3.2. **Linear viscoelasticity.** Consider now a linear viscoelastic material [37] under harmonic loading. For this type of loading, it is convenient to work in the frequency domain and adopt the representation

$$\boldsymbol{\varepsilon}(t) = \boldsymbol{\varepsilon}' \cos(\omega t) - \boldsymbol{\varepsilon}'' \sin(\omega t) = \mathrm{Re}[(\boldsymbol{\varepsilon}' + i\boldsymbol{\varepsilon}'')e^{i\omega t}], \tag{17}$$

where $\boldsymbol{\varepsilon}'$ and $\boldsymbol{\varepsilon}''$ are the real and imaginary parts of the complex representation of the harmonic strain and, similarly,

$$\boldsymbol{\sigma}(t) = \boldsymbol{\sigma}' \cos(\omega t) - \boldsymbol{\sigma}'' \sin(\omega t) = \mathrm{Re}[(\boldsymbol{\sigma}' + i\boldsymbol{\sigma}'')e^{i\omega t}]. \tag{18}$$

In this representation, a general viscoelastic material response can be expressed as [38, 39, 40]

$$\boldsymbol{\sigma}' + i\boldsymbol{\sigma}'' = (\mathbb{C}' + i\mathbb{C}'') : (\boldsymbol{\varepsilon}' + i\boldsymbol{\varepsilon}''), \tag{19}$$

where $\mathbb{C}' = \mathbb{C}_e$ and $\mathbb{C}'' = \omega\mathbb{C}_v$ are frequency-dependent storage and loss moduli, respectively.

We define the average dissipated energy as:

$$\phi(\boldsymbol{\varepsilon}', \boldsymbol{\varepsilon}'') = \frac{1}{2\pi}\,\mathrm{Im} \oint \boldsymbol{\sigma} : d\boldsymbol{\varepsilon} = \frac{1}{2}\left(\boldsymbol{\varepsilon}' : \mathbb{C}'' : \boldsymbol{\varepsilon}' + \boldsymbol{\varepsilon}'' : \mathbb{C}'' : \boldsymbol{\varepsilon}''\right), \tag{20}$$

and the average stored energy

$$W(\boldsymbol{\varepsilon}', \boldsymbol{\varepsilon}'') = \frac{1}{T}\,\mathrm{Re} \oint \boldsymbol{\sigma} : d\boldsymbol{\varepsilon} = \frac{1}{2}\left(\boldsymbol{\varepsilon}' : \mathbb{C}' : \boldsymbol{\varepsilon}' + \boldsymbol{\varepsilon}'' : \mathbb{C}' : \boldsymbol{\varepsilon}''\right). \tag{21}$$

Note that these energies cannot be used as potentials for the complex stress. Indeed, writing (19) in matrix form, we obtain

$$\begin{bmatrix} \boldsymbol{\sigma}' \\ \boldsymbol{\sigma}'' \end{bmatrix} = \begin{bmatrix} \mathbb{C}' & -\mathbb{C}'' \\ \mathbb{C}'' & \mathbb{C}' \end{bmatrix} \begin{bmatrix} \boldsymbol{\varepsilon}' \\ \boldsymbol{\varepsilon}'' \end{bmatrix} \tag{22}$$

and the antisymmetry of the constitutive matrix indicates the lack of a potential. The matrix can be made symmetric by reversing the sign of the second equation, but it then becomes negative-definite.

An alternative formulation can be obtained using complex, or Wirtinger [41], derivatives defined as

$$\frac{\partial F}{\partial \boldsymbol{\varepsilon}} = \frac{\partial F}{\partial \boldsymbol{\varepsilon}'} - i\frac{\partial F}{\partial \boldsymbol{\varepsilon}''}\,, \tag{23}$$

on functions $F(\boldsymbol{\varepsilon}', \boldsymbol{\varepsilon}'')$ of complex strain. Defining $F(\boldsymbol{\varepsilon}', \boldsymbol{\varepsilon}'')$ as

$$F(\boldsymbol{\varepsilon}', \boldsymbol{\varepsilon}'') = \frac{1}{2}\boldsymbol{\varepsilon}' : \mathbb{C}' : \boldsymbol{\varepsilon}' - \boldsymbol{\varepsilon}' : \mathbb{C}'' : \boldsymbol{\varepsilon}'' - \frac{1}{2}\boldsymbol{\varepsilon}'' : \mathbb{C}' : \boldsymbol{\varepsilon}'' = \frac{1}{2}\begin{bmatrix} \boldsymbol{\varepsilon}' & \boldsymbol{\varepsilon}'' \end{bmatrix} \begin{bmatrix} \mathbb{C}' & -\mathbb{C}'' \\ -\mathbb{C}'' & -\mathbb{C}' \end{bmatrix} \begin{bmatrix} \boldsymbol{\varepsilon}' \\ \boldsymbol{\sigma}'' \end{bmatrix}. \tag{24}$$

We can formally write

$$\boldsymbol{\sigma} = \boldsymbol{\sigma}' + i\boldsymbol{\sigma}'' = \frac{\partial F}{\partial \boldsymbol{\varepsilon}}(\boldsymbol{\varepsilon}), \tag{25}$$

where $\boldsymbol{\varepsilon} = \boldsymbol{\varepsilon}' + i\boldsymbol{\varepsilon}''$. Similarly, we can define a conjugate function $F^*(\boldsymbol{\sigma}', \boldsymbol{\sigma}'')$:

$$F^*(\boldsymbol{\sigma}', \boldsymbol{\sigma}'') = \frac{1}{2}\begin{bmatrix}\boldsymbol{\sigma}' & \boldsymbol{\sigma}''\end{bmatrix}\begin{bmatrix}(\mathbb{C}' + \mathbb{C}'' : \mathbb{C}'^{-1} : \mathbb{C}'')^{-1} & (\mathbb{C}'' + \mathbb{C}' : \mathbb{C}''^{-1} : \mathbb{C}')^{-1} \\ (\mathbb{C}'' + \mathbb{C}' : \mathbb{C}''^{-1} : \mathbb{C}')^{-1} & -(\mathbb{C}' + \mathbb{C}'' : \mathbb{C}'^{-1} : \mathbb{C}'')^{-1}\end{bmatrix}\begin{bmatrix}\boldsymbol{\sigma}' \\ \boldsymbol{\sigma}''\end{bmatrix}, \tag{26}$$

using which we can write

$$\boldsymbol{\varepsilon} = \boldsymbol{\varepsilon}' + i\boldsymbol{\varepsilon}'' = \frac{\partial F^*}{\partial \boldsymbol{\sigma}}(\boldsymbol{\sigma}), \tag{27}$$

where $\boldsymbol{\sigma} = \boldsymbol{\sigma}' + i\boldsymbol{\sigma}''$ and the derivative is a Wirtinger derivative. However, it can be readily verified that these functions are not convex in the imaginary parts of strain and stress, and a constitutive gap function cannot be directly constructed from them.

Cherkaev and Gibiansky [28] introduced "mixed" functions, which can lead to minimization principles. The first mixed potential is defined as

$$W_{\epsilon\sigma}(\boldsymbol{\varepsilon}', \boldsymbol{\sigma}'') = \frac{1}{2}\begin{bmatrix}\boldsymbol{\varepsilon}' & \boldsymbol{\sigma}''\end{bmatrix}\begin{bmatrix}\mathbb{C}' + \mathbb{C}'' : \mathbb{C}'^{-1} : \mathbb{C}'' & -\mathbb{C}'' : \mathbb{C}'^{-1} \\ -\mathbb{C}'^{-1} : \mathbb{C}'' & \mathbb{C}'^{-1}\end{bmatrix}\begin{bmatrix}\boldsymbol{\varepsilon}' \\ \boldsymbol{\sigma}''\end{bmatrix}. \tag{28}$$

This, in turn, renders

$$\boldsymbol{\sigma}' = \partial_{\boldsymbol{\varepsilon}'} W_{\epsilon\sigma}(\boldsymbol{\varepsilon}', \boldsymbol{\sigma}''), \tag{29}$$

and

$$\boldsymbol{\varepsilon}'' = \partial_{\boldsymbol{\sigma}''} W_{\epsilon\sigma}(\boldsymbol{\varepsilon}', \boldsymbol{\sigma}''). \tag{30}$$

The dual potential can be written then:

$$W_{\sigma\epsilon}(\boldsymbol{\sigma}', \boldsymbol{\varepsilon}'') = \frac{1}{2}\begin{bmatrix}\boldsymbol{\sigma}' & \boldsymbol{\varepsilon}''\end{bmatrix}\begin{bmatrix}\mathbb{C}'^{-1} & \mathbb{C}'^{-1} : \mathbb{C}'' \\ \mathbb{C}'' : \mathbb{C}'^{-1} & \mathbb{C}' + \mathbb{C}'' : \mathbb{C}'^{-1} : \mathbb{C}''\end{bmatrix}\begin{bmatrix}\boldsymbol{\sigma}' \\ \boldsymbol{\varepsilon}''\end{bmatrix} \tag{31}$$

such that

$$\boldsymbol{\varepsilon}' = \partial_{\boldsymbol{\sigma}'} W_{\sigma\epsilon}(\boldsymbol{\sigma}', \boldsymbol{\varepsilon}''), \tag{32}$$

and

$$\boldsymbol{\sigma}'' = \partial_{\boldsymbol{\varepsilon}''} W_{\sigma\epsilon}(\boldsymbol{\sigma}', \boldsymbol{\varepsilon}''). \tag{33}$$

It is then possible to define a constitutive gap function as

$$G(\boldsymbol{\varepsilon}', \boldsymbol{\varepsilon}'', \boldsymbol{\sigma}', \boldsymbol{\sigma}'') = W_{\epsilon\sigma}(\boldsymbol{\varepsilon}', \boldsymbol{\sigma}'') + W_{\sigma\epsilon}(\boldsymbol{\sigma}', \boldsymbol{\varepsilon}'') - (\boldsymbol{\sigma}' : \boldsymbol{\varepsilon}' + \boldsymbol{\sigma}'' : \boldsymbol{\varepsilon}'') \tag{34}$$

which is convex and has the sought properties

$$G(\boldsymbol{\varepsilon}', \boldsymbol{\varepsilon}'', \boldsymbol{\sigma}', \boldsymbol{\sigma}'') \geq 0 \quad \text{and} \quad G(\boldsymbol{\varepsilon}', \boldsymbol{\varepsilon}'', \boldsymbol{\sigma}', \boldsymbol{\sigma}'') = 0 \iff (19)\,. \tag{35}$$

Note that Cherkaev and Gibiansky [28] also identified that functions (24) and (26) lead to saddle-point (min-max) formulations. In this case, the parameters are the storage and loss moduli.

3.3. **Material identification algorithm.** Let us revisit the identification problem (9) with the distance function (34) then, where parameters p are complex moduli. In the following, we will consider the case where we postulate the existence of N phases, each characterized by a complex modulus $\mathbb{C}_i$, $i \in \{1, 2, \cdots, N\}$. If we apply the equilibrium constraint by way of a complex Lagrange multiplier field $\boldsymbol{\eta}$, stationnarity conditions on stress fields $\boldsymbol{\sigma}'$ and $\boldsymbol{\sigma}''$ yield (for $e \in \{1, 2, \cdots, M\}$)

$$\boldsymbol{\sigma}'_e = \mathbb{C}'_{i_e} : \boldsymbol{\varepsilon}'_e - \mathbb{C}''_{i_e} : \boldsymbol{\varepsilon}''_e + \mathbb{C}'_{i_e} : (\mathbf{B}_e \boldsymbol{\eta}'), \tag{36a}$$

$$\boldsymbol{\sigma}''_e = \mathbb{C}''_{i_e} : \boldsymbol{\varepsilon}'_e + \mathbb{C}'_{i_e} : \boldsymbol{\varepsilon}''_e + \mathbb{C}'_{i_e} : (\mathbf{B}_e \boldsymbol{\eta}''), \tag{36b}$$

where i_e denotes the current mapping of material point e to phase i. Introducing these relations in the balance equation yields in turn

$$\left(\sum_{e=1}^{M} w_e \mathbf{B}_e^T \mathbb{C}'_{i_e} \mathbf{B}_e \right) \boldsymbol{\eta} = \boldsymbol{f} - \sum_{e=1}^{M} w_e \mathbf{B}_e^T \mathbb{C}_{i_e} : (\mathbf{B}_e \boldsymbol{u}_{\text{exp}}), \tag{37}$$

which can be solved for $\boldsymbol{\eta}$.

The minimization problem can be written as the following

$$\inf_{\mathbb{C}_i, i_e} \sum_{e=1}^{M} w_e G(\mathbf{B}_e \boldsymbol{u}_{\text{exp}}, \boldsymbol{\sigma}_e; \mathbb{C}_{i_e}). \tag{38}$$

We solve this optimization problem with recourse to k-planes clustering [35], where in an alternating sequence of assigning clusters and principal component analysis' steps, one can partition data points and assign a plane to each partition. This framework is among the most efficient existing plane clustering techniques that is also robust to presence of noise [36]. We have delineated the procedure used here in algorithm 1.

Algorithm 1 k-planes clustering algorithm

1: **Require**: set of mechanical data $\{\boldsymbol{z}_e = (\boldsymbol{\varepsilon}_e, \boldsymbol{\sigma}_e)\}_{e=1}^{M}$, weights $\{w_e\}_{e=1}^{M}$. Choose a number of planes N.
2: **Initialization**: initialize hyperplanes' tensors $\mathbb{C}_i^0$, $i \in \{1, \cdots, N\}$ (from arbitrary first guess or from a previous run)
3: **Clustering**: set $r = 0$
   (a) find optimal mapping
   $$I^r(e) = \arg\min_i G(\boldsymbol{\varepsilon}_e, \boldsymbol{\sigma}_e; \mathbb{C}_i^r) \quad e = 1, \ldots, M$$
   (b) update hyperplanes' tensors
   $$\mathbb{C}_i^{r+1} = \arg\min_{\mathbb{C}} \sum_{e: I^r(e) = i} w_e G(\boldsymbol{\varepsilon}_e, \boldsymbol{\sigma}_e; \mathbb{C}) \quad i = 1, \ldots, N$$
   (c) **if** $\mathbb{C}_i^{r+1} = \mathbb{C}_i^r$, $i = 1, \ldots, N$ and $I^r = I^{r-1}$ (for $r > 0$) : **exit**
   (d) $r \leftarrow r + 1$; **goto** (a)

The material identification problem can then be solved by alternating between k-planes clustering and solving equilibrium equations (37). This process is outlined in algorithm 2, where $\hat{d}^r$ denotes the total constitutive gap:

$$\hat{d}^r = \sum_{e=1}^{M} w_e G(\mathbf{B}_e \boldsymbol{u}_{\text{exp}}, \boldsymbol{\sigma}_e^r; \mathbb{C}_{I^r(e)}^r)$$

where G corresponds to (34), or alternatively (15) if the material is known to be elastic.

Algorithm 2 Material identification for a heterogeneous medium

1: **Require:** strain data set $\{\boldsymbol{\varepsilon}_e\}_{e=1}^M$ where M is the number of material points, discrete gradient matrix $\mathbf{B}$, material point weights $\mathbf{W} = \text{diag}(w_e, e \in \{1, \cdots, M\})$, applied force vector $\mathbf{f}$. Pick an initial guess for the number of phases N. Choose tolerance *tol*.
2: **Initialization:** Set $r = 0$. Choose N random hyperplanes $\{\mathbb{C}_i^r, i \in \{1, \cdots, N\}\}$. Initialize hyperplane assignment $I^r(e), e = 1, \ldots, M$.
3: **Alternated minimization**:
   (a) stress update (37) and (36) $\longrightarrow \{\boldsymbol{\sigma}_e^{r+1}, e = 1, \ldots, M\}$
   (b) k-planes clustering (38) $\longrightarrow I^{r+1}$, $\mathbb{C}_i^{r+1}$ $(i = 1, \ldots, N)$, $\hat{d}^{r+1}$
   (c) convergence: **if** $|\hat{d}^{r+1} - \hat{d}^r| < tol$ **and** $I^{r+1} = I^r$: **break**
   (d) $r \leftarrow r + 1$; **goto** (a)

Note that algorithm 2 requires to pick a number of phases N. It can either be guessed, e.g. from a first identification stage as in the examples below, or otherwise iteratively determined by an elbow method (i.e. increasing N until observing no significant improvement in the minimum distance reached).

4. Model-free constitutive gap

The above constitutive gap functions rely on the postulate of a specific linear model in elasticity or viscoelasticity. But the choice of a specific model introduces a bias in the identification process. Model-free representation of the constitutive response in linear elastic and viscoelastic media [42, 43] has been emerging as a data-driven approach that is based on a given set of N stress-strain pairs

$$\mathcal{D} = \{\hat{\boldsymbol{z}}_\alpha = (\hat{\boldsymbol{\varepsilon}}_\alpha, \hat{\boldsymbol{\sigma}}_\alpha), \alpha = 1, \ldots, N\} \tag{39}$$

coming from experimental tests or other source. Introducing the constitutive distance $d(\boldsymbol{z}, \hat{\boldsymbol{z}})$ as

$$\begin{aligned} d(\boldsymbol{z}, \hat{\boldsymbol{z}}; \mathbb{C}) &= \frac{1}{2} \|\boldsymbol{z} - \hat{\boldsymbol{z}}\|_{\mathbb{C}}^2 \\ &= \frac{1}{2} \left((\boldsymbol{\varepsilon} - \hat{\boldsymbol{\varepsilon}}) : \mathbb{C} : (\boldsymbol{\varepsilon} - \hat{\boldsymbol{\varepsilon}}) + (\boldsymbol{\sigma} - \hat{\boldsymbol{\sigma}}) : \mathbb{C}^{-1} : (\boldsymbol{\sigma} - \hat{\boldsymbol{\sigma}}) \right) \end{aligned} \tag{40}$$

where $\mathbb{C}$ is a (real-valued) fourth-order tensor acting as a metric, where $\mathbb{C}$ practically serves as a normalization parameter, and while it can take arbitrary values, it can be judiciously chosen based on a preliminary analysis of the constitutive data, e.g. through a principal component analysis [44]. One can then define the distance between a material state $\boldsymbol{z} = (\boldsymbol{\varepsilon}, \boldsymbol{\sigma})$ and the data set $\mathcal{D}$:

$$d_{\mathcal{D}}(\boldsymbol{z}; \mathbb{C}) = \min_{\alpha=1,\dots,N} d(\boldsymbol{z}, \hat{\boldsymbol{z}}_\alpha; \mathbb{C}). \tag{41}$$

Note that, if strains and stress tensors are complex, as in the harmonic viscoelastic case, the inner product in the distance should be understood as the Hermitian scalar product. As demonstrated in [45, 31], when the data set converges towards a constitutive model, the above distance actually converges towards the associated constitutive gap. We can thus use distance (41) as a model-free constitutive gap function, parameterized by N stress-strain pairs and a metric: $p = \{\mathbb{C}, \hat{\boldsymbol{z}}_\alpha, \alpha = 1, \dots, N\}$ and

$$G(\boldsymbol{\varepsilon}, \boldsymbol{\sigma}; p) = d_{\mathcal{D}}(\boldsymbol{z} = (\boldsymbol{\varepsilon}, \boldsymbol{\sigma}); \mathbb{C}). \tag{42}$$

Note that we keep the notation G for the constitutive gap, but that it corresponds, in the model-free case, to a different expression than in the model-based case of the previous section.

4.1. **Model-free material identification algorithm.** Considering the distance (41), the identification problem (9) takes a specific form, where parameters p are the set of data points $p = \{\hat{\boldsymbol{z}}_\alpha, \alpha = 1, \dots, N\}$ if we consider the metric as a given hyper-parameter. Applying the equilibrium constraint by way of a Lagrange multiplier field $\boldsymbol{\eta}$, stationnarity conditions on stress field $\boldsymbol{\sigma}$ and $\boldsymbol{\eta}$ yield [17]:

$$\sum_{e=1}^{M} w_e \mathbf{B}_e^T \mathbb{C} \mathbf{B}_e \boldsymbol{\eta} = \mathbf{f} - \sum_{e=1}^{M} w_e \mathbf{B}_e^T \hat{\boldsymbol{\sigma}}_{\alpha_e} \tag{43a}$$

$$\boldsymbol{\sigma}_e = \hat{\boldsymbol{\sigma}}_{\alpha_e} + \mathbb{C} \mathbf{B}_e \boldsymbol{\eta} \quad e = 1, \dots, M \tag{43b}$$

where the first equation is a linear system in $\boldsymbol{\eta}$, while the second provides an update rule for the stresses. The minimization with respect to $\hat{\boldsymbol{z}}_\alpha$ ($\alpha = 1, \dots, N$) and α_e ($e = 1, \dots, M$)

$$\min_{\{\hat{\boldsymbol{z}}_\alpha, \alpha \in [1,N]\}, \{\alpha_e, e \in [1,M]\}} \sum_{e=1}^{M} w_e G(\mathbf{B}_e \mathbf{u}_{\text{exp}}, \boldsymbol{\sigma}_e; \hat{\boldsymbol{z}}_{\alpha_e}) \tag{44}$$

can be solved by way of a k-means algorithm, for example. The overall problem can then be solved by an alternated minimization scheme, repeating (43) and (44) until convergence (algorithm 3). The unicity of solutions provided by this data-driven identification (DDI) algorithm mostly depend on the ratio N/M, as shown in recent studies [46, 47].

As noted above, in the harmonic viscoelastic case, the above model-free constitutive gap (42) can be used with a real metric $\mathbb{C}$. The use of mixed quadratic forms $W_{\varepsilon\sigma}$ and $W_{\sigma\varepsilon}$, which would imply to introduce additional

algorithmic hyper-parameters, is not necessary. In the time-domain, not considered here, previous strains and stresses should be included in the data space, as shown in [48].

Algorithm 3 Data-driven identification for a heterogeneous medium

1: **Require:** Strain data set $\{\boldsymbol{\varepsilon}_e\}_{e=1}^M$ where M is the number of material points, discrete gradient matrix $\mathbf{B}$, material point weights $\mathbf{W} = \text{diag}(w_e, e = 1, \dots, M)$, applied force vector $\mathbf{f}$. Choose tolerance *tol*.
2: **Initialization:** Initialize stresses $\{\boldsymbol{\sigma}_e\}_{e=1}^M$ (e.g. to zero values). Set $r = 0$. Initialize clustering (44) $\longrightarrow \mathbb{I}^r$, $\{\hat{\boldsymbol{z}}_\alpha^r, \alpha \in [1, N]\}$, d^r
3: **Alternated minimization**:
   (a) stress update (43) $\longrightarrow \{\boldsymbol{\sigma}_e^{r+1}, e \in [1, M]\}$
   (b) k-means clustering (44) $\longrightarrow \mathbb{I}^{r+1}$, $\{\hat{\boldsymbol{z}}_\alpha^{r+1}, \alpha \in [1, N]\}$, d^{r+1}
   (c) convergence: **if** $|d^{r+1} - d^r| < tol$ **and** $\mathbb{I}^{r+1} = \mathbb{I}^r$: **break**
   (d) $r \leftarrow r + 1$; **goto** (a)

5. Numerical applications

In this section, we will validate our proposed numerical algorithms by investigating composite domains comprised of matrix and inclusions. We will proceed with the method of *manufactured solutions* where we solve forward problems for prescribed domains and boundary conditions. The resultant displacement fields are then used as data input for our identification schemes. Motivated by biomedical applications, in particular elastography [6, 49, 50] techniques, we will only focus on identifying heterogeneous shear moduli in our numerical examples. Inspired by examples considered in [50], we will consider examples involving pure transverse shear, as detailed below.

5.1. **Numerical setting.** We will illustrate the methodology on two dimensional problems, considering transverse shear only. Our computational experiments are inspired by tumor detection application in biomedical fields, where boundary measurements are used to detect and identify a stiff region that reflects tumor inside a soft healthy tissue [51, 52].The governing equations in the frequency domain are:

$$\boldsymbol{\nabla} \cdot \boldsymbol{\sigma} - \rho(x)\omega^2 \boldsymbol{u}(x) = 0, \tag{45}$$

where we assume absence of body forces. The displacement field is then assumed to be of the form $\boldsymbol{u}(x, y, t) = w(x, y, t)\boldsymbol{e}_z$, resulting in pure shear strain states. By further assuming an isotropic response in the $x - y$ plane, this yields pure shear stress states, with

$$\sigma'_{xz} + i\sigma''_{xz} = (\mu' + i\mu'')(w'_x + iw''_x), \tag{46a}$$

$$\sigma'_{yz} + i\sigma''_{yz} = (\mu' + i\mu'')(w'_y + iw''_y), \tag{46b}$$

where μ' and μ'' are the storage and loss shear moduli, respectively. The momentum balance equation then writes under the form of:

$$(\mu' + i\mu'')(\Delta w' + i\Delta w'') = \rho\omega^2(w' + iw''). \tag{47}$$

We will consider heterogeneous samples, where the complex shear modulus varies from one phase to another.

5.1.1. *Methodology.* In the examples below, we validate the identification algorithm on synthetic data. Virtual two-phase specimens, composed of inclusions embedded in a matrix, are subject to harmonic loads applied on their boundaries. Time-harmonic complex displacement fields are then generated by solving the forward elastodynamic problem using assigned complex shear moduli for each phase. We then discard the moduli and provide only these displacement fields to the identification procedure, which estimates (i) the phase morphology (spatial distribution) and (ii) the local complex moduli of each phase. Because the data are manufactured with known parameters, the recovered morphology and properties can be compared directly against ground truth to quantify accuracy.

5.1.2. *Implementation.* The algorithms described above were implemented in python, using SciPy sparse linear algebra solvers [53], and Scikit-learn [54] for clustering. The DDI step involves a unique factorization, associated to the pseudo-elasticity problem (43). The associated computational cost is thus marginal. The main computational cost is thus associated to the repeated clustering step, itself linked to the number of material (i.e. integration) points and the number of clusters, typically one or two orders of magnitude lower. The k-planes clustering phase involves solving repeated linear elasticity problems (in real or complex numbers). The stiffness matrix can nonetheless be pre-factored, since its sparsity pattern will not change. The computational cost of this phase is thus linked to the number of degrees of freedom (i.e. number of nodes of the spatial discretization used).

5.2. **Case I: Elastic inclusions and elastic matrix.** The sample cross-section in this case is a square with length of 0.1 meter, subjected to harmonic traction boundary conditions applied at 1000 Hz (see Fig. 1). There are three cylindrical inclusions, which can relatively easily be spotted from displacement amplitude maps (see figures 2 and 6). These inclusions are elastic, with a shear modulus $\mu_i = 10$ kPa, for both subcases considered below. A density $\rho = 1000$ kg/m^3 has been used for both phases.

This case is a fully elastic material, i.e. the matrix exhibits an elastic response as well, with a shear modulus $\mu_m = 1$ kPa. We are thus in the configuration of hard inclusions in a soft matrix. The specific boundary conditions are illustrated in figure 1: the bottom side is completely blocked, the top side is loaded uniformly (shear amplitude of 1 kPa), while the lateral sides are left free. Note that, if we are using a precise description of this loading in the DDI identification below, this could alternatively be bypassed

by eliminating the boundary degrees of freedom in cases where the loading is unknown or not precisely known. Indeed, in the harmonic context, inertia forces are computed directly from the complex displacement amplitude field, which is thus sufficient to write equilibrium equations inside the domain. Equilibrium at the boundaries can also be treated globally, as shown in [20].

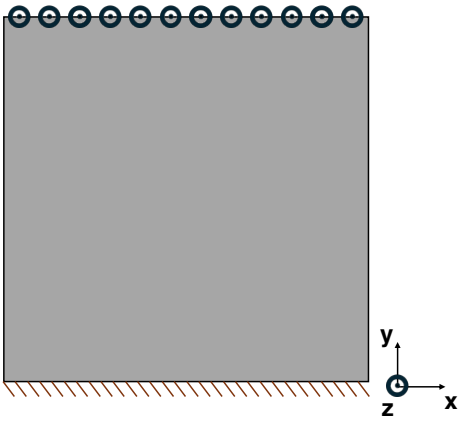

FIGURE 1. Schematics representing boundary conditions for case I.

The map of harmonic displacement amplitude resulting from this loading is shown in figure 2. It has been computed on a fine mesh (79 360 triangular elements) providing enough resolution compared to wavelengths in the matrix.

The DDI identification algorithm 3 has been applied to this displacement field, considering the loading as known, yielding a cloud of shear strain-stress pairs, shown on figure 3. Each point corresponds to one of the shear components at a material point (in this case, centroids of elements). The metric used in the constitutive distance (40) corresponds to a shear modulus $\mu = 2$ kPa. Qualitatively, it is quite clear to recognize that there are (at least) two distinct material responses, despite the presence of noise and outliers. The number of outliers could be reduced by tuning the metric and the number of clusters (chosen here as $N = M/50 = 1587$), but such optimization will not be pursued here, since we will apply further k-planes clustering.

In order to classify the data points in two groups, we can then apply algorithm 1, yielding the two planes represented by purple dashed lines on figure 3. Planes corresponding to the reference material are shown as red dotted line for comparison. Numerically, the values obtained are the

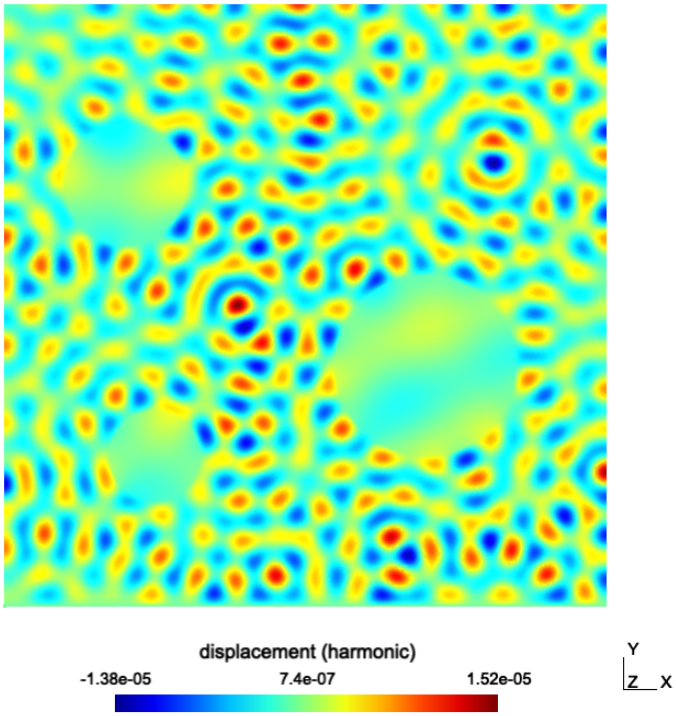

FIGURE 2. Harmonic displacement amplitude map for case I (purely elastic) used as input data for the identification algorithm.

following:

$$\tilde{\mu}_m = 1.007\,\text{kPa} \quad , \quad \tilde{\mu}_i = 9.058\,\text{kPa}$$

showing a good agreement with reference values (shown in red on figure 3).

Through the k-plane clustering, each material point is associated to one of the planes, and thus to a shear modulus value. Once represented spatially, this mapping provides a view of the sample morphology (i.e. distribution of phases), shown in figure 4 (each element of the background mesh has been coloured by its associated modulus amplitude).

We see that the cylindrical inclusions are well captured. A few elements have been misclassified, with respect to the reference solution, but the agreement is very satisfactory.

5.3. **Case II: Elastic inclusions and viscoelastic matrix.** Next, we consider the case of the same elastic inclusions, but embedded in a viscoelastic matrix, characterized by a complex shear modulus $\mu_m = (1 + 0.1i)$ kPa. In order to obtain a better signal in the displacement amplitude map, the loading has been modified: lateral sides are now loaded as well, with a linear distribution of harmonic shear, spatially ramped between 0 and 1

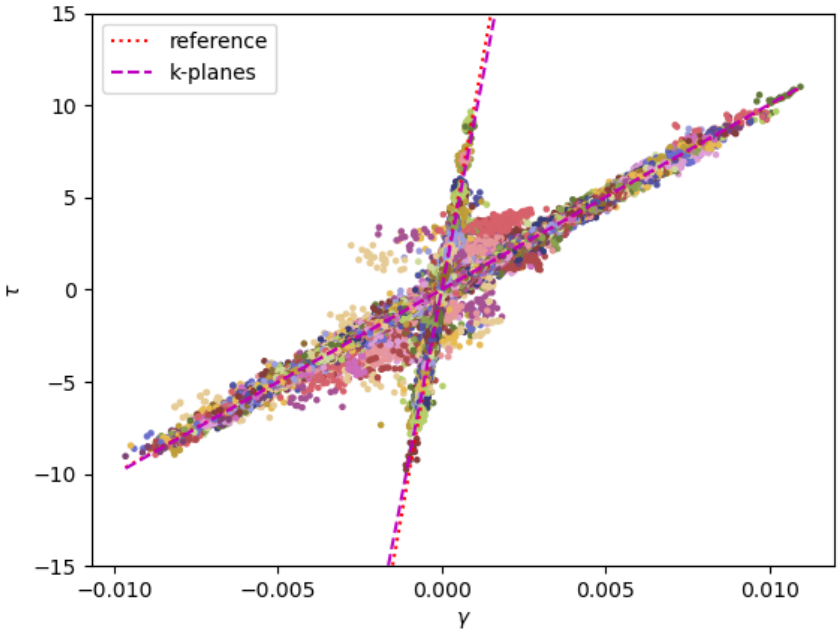

FIGURE 3. Shear stress–strain data from identification for the purely elastic case I: Points are DDI outputs (cluster colors); purple dashed lines show k-planes; red dotted line shows the reference constitutive response.

kPa, and at a phase difference of $\pi/2$ with respect to the top loading (see Fig. 5). This loading was chosen to ensure a sufficient signal (i.e. displacement amplitude) in the lower part of the sample, despite the damping in the viscoelastic matrix.

Given the viscoelastic nature of the matrix, the harmonic displacement field used as input is now complex: figure 6 shows its real and imaginary parts. It has been computed on the same mesh as in the previous example (79 360 triangular elements).

The DDI identification algorithm 3 can be applied to these data, using complex numbers. It yields a cloud of complex strain-stress pairs: figure 7 shows this cloud, projected in the space of strain and stress amplitudes. The dispersion is more marked than previously. As indicated before, this dispersion depends (among other parameters) on the choice of the distance metric, which was taken here at $\mu = 5$ kPa. The number of outliers also depends on the number of clusters (chosen here as $N = M/60 = 1322$).

In order to classify the data points in two groups, we can then apply algorithm 1, yielding the two (hyper-)planes represented by purple dashed lines on figure 7. These planes actually lie in a four-dimensional space, and

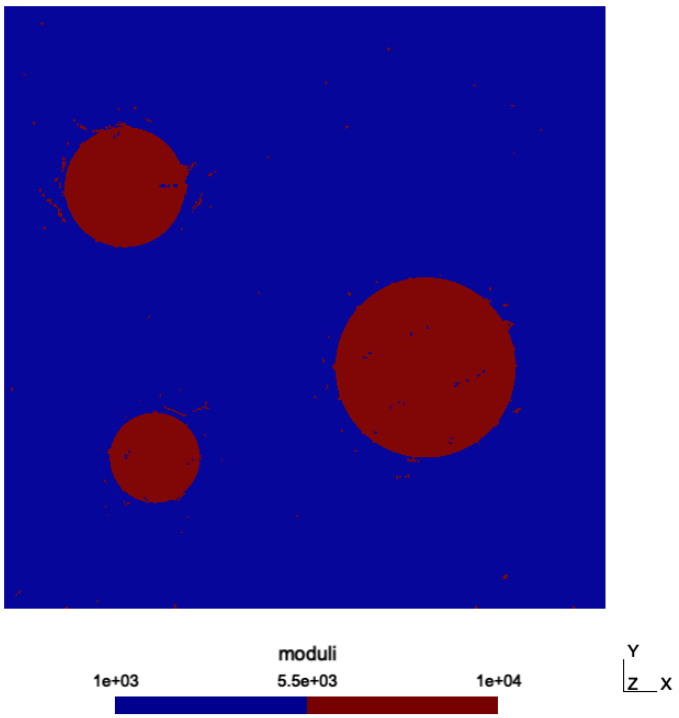

FIGURE 4. Identified shear moduli for the purely elastic case I.

relate complex strain and stress amplitudes. The associated complex moduli are the following:

$$\tilde{\mu}_m = 1.017 + 0.1i\,\text{kPa} \quad , \quad \tilde{\mu}_i = 9.487\,\text{kPa}$$

showing a good agreement with reference values (shown in red on figure 7).

Through the k-plane clustering, each material point is associated to one of the planes, and thus to a (complex) shear modulus value. As in the previous example, we can thus build a view of the sample morphology (i.e. distribution of phases), shown in figure 8 (each element of the background mesh has been colored by its associated modulus amplitude).

We see that the cylindrical inclusions are again well captured. A few elements have been misclassified, with respect to the reference solution, but the agreement is still very satisfactory.

5.4. **Case III: Viscoelastic inclusions and viscoelastic matrix.** In our third numerical experiment, we consider a sample with a different geometry, loading, and material properties. The sample cross-section in this second case is a square with length of 0.04 meter, subjected to harmonic traction boundary conditions applied at 500 Hz. The distribution of these boundary conditions corresponds to the second case (see Fig. 5). In this example,

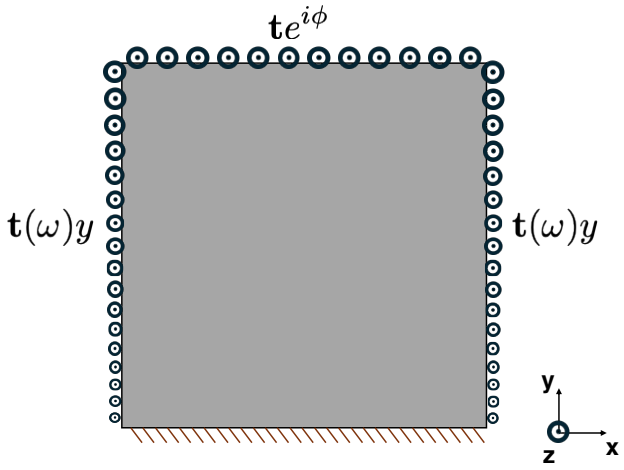

FIGURE 5. Schematics representing boundary conditions for case II and III.

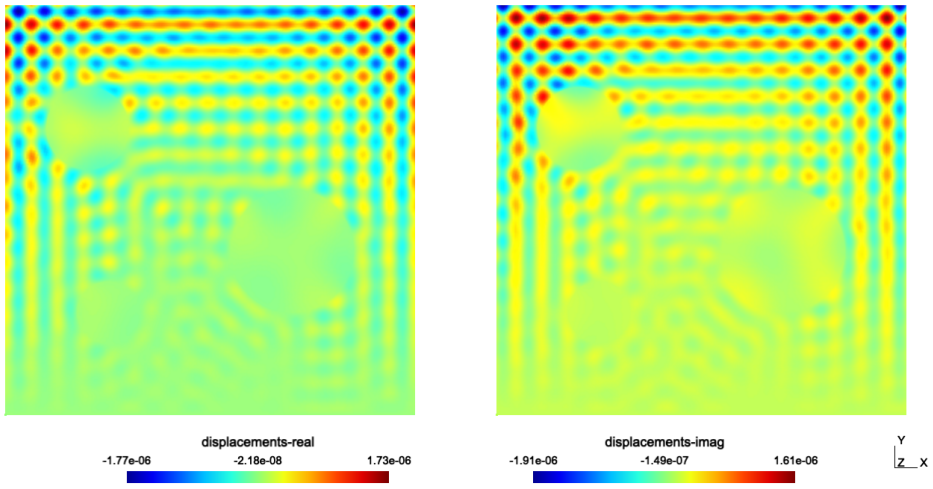

FIGURE 6. Complex displacement amplitude map for case II (elastic inclusion with viscoelastic matrix) used as input data for the identification algorithm.

there is a single inclusion of elliptic shape in the matrix, and both phases are considered as viscoelastic. Complex moduli used to generate the harmonic displacement fields are chosen as follows:

$$\mu_m = 5.0 + 2.5i\,\text{kPa} \quad , \quad \mu_i = 20.0 + 10.0i\,\text{kPa}$$

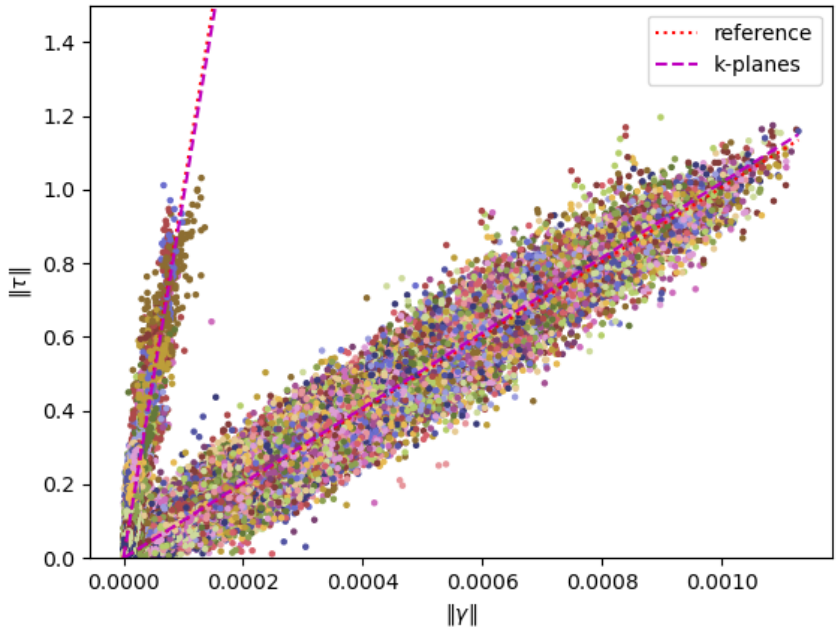

FIGURE 7. Shear stress–strain data from identification for case II with elastic inclusions and viscoelastic matrix: Points are DDI outputs (cluster colors); purple dashed lines show k-planes; red dotted line shows the reference constitutive response.

yielding the maps shown in figure 9 (results obtained with a mesh of 15473 nodes and 30488 triangular elements). Note that, it is more difficult to guess, from these maps, the sample morphology than it was for the first sample. We can also note that the mesh used in this case is a bit coarser than in the previous ones, reflecting the difference in spatial characteristic length between them.

Application of the standard DDI method (algorithm 3, with a metric $\mu =$ 20 kPa and $N = M/60 = 508$ clusters) yields the cloud of (complex) strain-stress points shown in figure 10 (actually showing amplitude of complex strain and stress values). The data obtained is much more noisy than in previous examples (again, the result depends on the choice of metric and number of clusters). It is nonetheless possible to identify two subgroups by using the k-planes algorithm 1, represented by the two purple dashed lines in figure 10. These planes correspond to the following estimation of complex shear moduli:

$$\tilde{\mu}_m = 5.199 + 2.555i\,\text{kPa} \quad , \quad \tilde{\mu}_i = 14.705 + 6.763i\,\text{kPa}$$

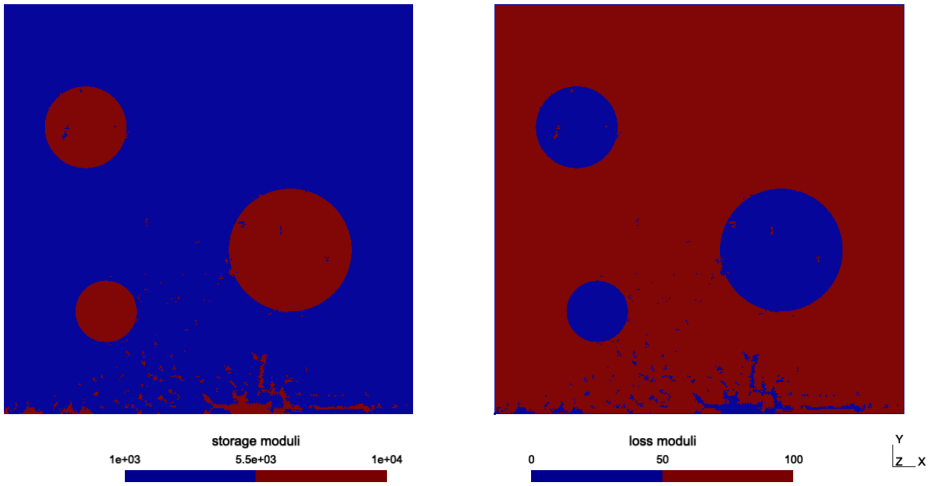

FIGURE 8. Identified storage and loss shear moduli for case II with elastic inclusions and viscoelastic matrix.

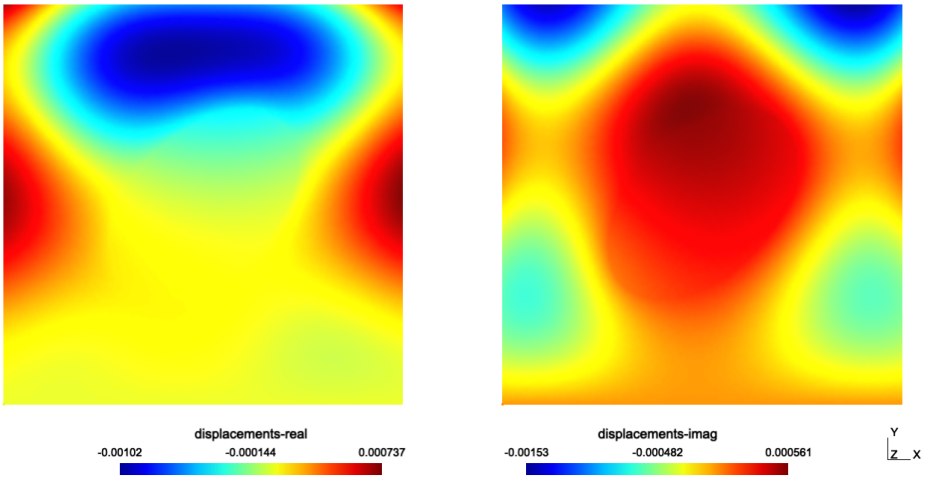

FIGURE 9. Complex displacement amplitude map for case III (viscoelastic inclusion with viscoelastic matrix) used as input data for the identification algorithm.

and we can see that the method fails to accurately approach the reference values (shown as red dashed lines in figure 10). If the agreement is reasonable for the softer (matrix) phase, the estimation is significantly off for the stiffer (inclusion) phase.

The k-plane clustering illustrated above can nonetheless be used as a first iteration of the material identification algorithm discussed in section 3.3

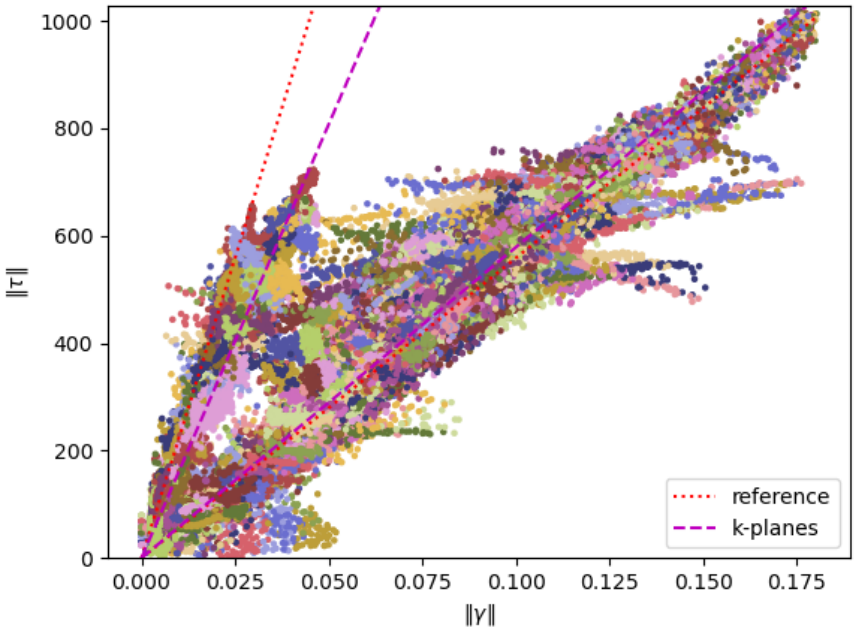

FIGURE 10. Shear stress–strain data from identification for case III with viscoelastic inclusions and viscoelastic matrix: Points are DDI outputs (cluster colors); purple dashed lines show k-planes; red dotted line shows the reference constitutive response.

(algorithm 2). Further application of this algorithm yields a much better estimation of the complex moduli of both phases, as illustrated in Figure 11. Actual values of estimated shear moduli are as follows:

$$\tilde{\mu}_m = 5.001 + 2.501i\,\text{kPa} \quad , \quad \tilde{\mu}_i = 19.371 + 9.463i\,\text{kPa}$$

which is much closer to reference values than after the first iteration. Note that application of algorithm 2 with a random initialization does not yield satisfactory results, confirming observations in the literature that k-planes clustering is very sensitive to initialization.

Finally, by looking at which phase each material point is associated, the morphology of the sample can be reconstructed, as shown in Figure 12. The elliptical inclusion is well caught, with only a few elements in the matrix being mistakenly be associated with the inclusion.

5.5. **Discussion.** Table 1 summarizes the values of reference and identified shear moduli, with the associated relative errors. We observe that these errors remain below 10%. We can also note that errors are systematically higher in inclusions than in the matrix. This can probably be interpreted as

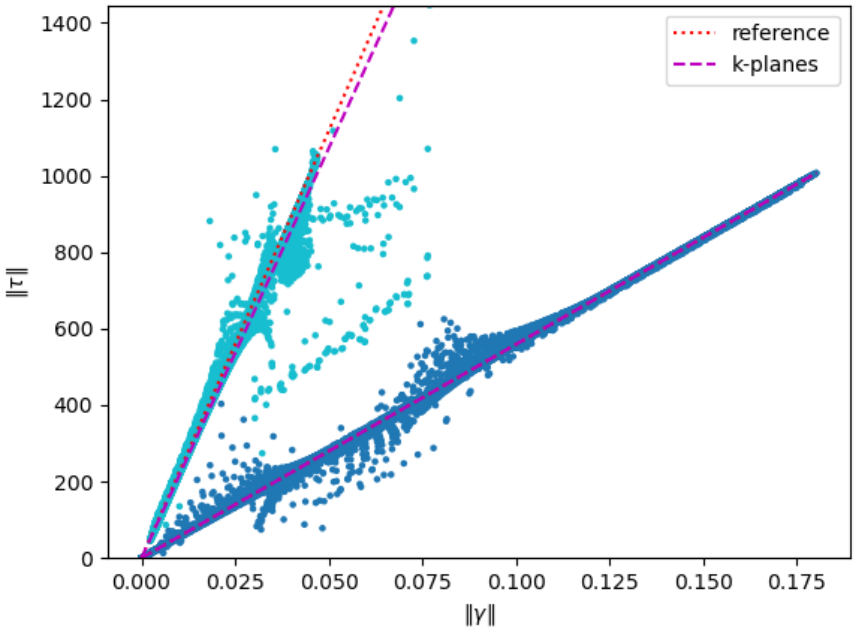

FIGURE 11. Shear stress-strain (amplitudes) data for case III obtained by k-planes identification (algorithm 2: data points (colours correspond to clusters), final k-planes (purple dashed lines), reference material (red dotted lines)

follows: input fields are typically smoother in the inclusions, providing less diverse information for the identification process which is based on clustering.

Regarding the prediction of phase morphology, we have listed in Table 2 the number of misclassified elements, i.e. for which the wrong phase was assigned. These numbers show that the assignment error is of the order of 0.5% to 1% in the first two cases, and less than 0.5% in the last case. From Figures 4, 8 and 12, we also see that these errors tend to appear around boundaries and interfaces, which is not so surprising.

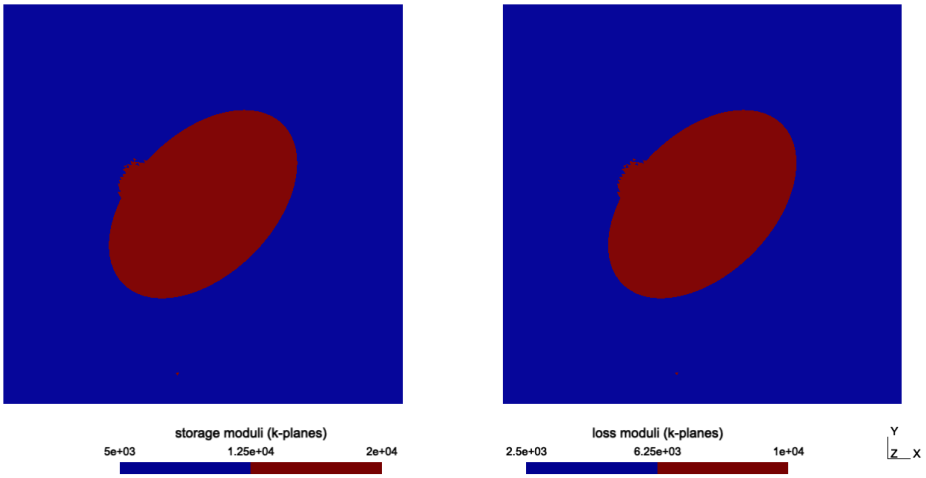

FIGURE 12. Identified storage and loss shear moduli for case III with viscoelastic inclusions and viscoelastic matrix.

TABLE 1. Summary of reference and identified moduli, for the different cases considered, with associated relative errors.

Moduli	Case I	Case II	Case III
Re$[\mu_m]$ [kPa]	1.000	1.000	5.000
Im$[\mu_m]$ [kPa]	-	0.100	2.500
Re$[\mu_i]$ [kPa]	10.000	10.000	20.000
Im$[\mu_i]$ [kPa]	-	-	10.000
Re$[\tilde{\mu}_m]$ [kPa]	1.007	1.017	5.001
Im$[\tilde{\mu}_m]$ [kPa]	-	0.100	2.501
Re$[\tilde{\mu}_i]$ [kPa]	9.058	9.487	19.371
Im$[\tilde{\mu}_i]$ [kPa]	-	-	9.463
err(Re$[\tilde{\mu}_m]$)	0.7%	1.7%	0.02%
err(Im$[\tilde{\mu}_m]$)	-	0.0%	0.04%
err(Re$[\tilde{\mu}_i]$)	9.4%	5.1%	3.1%
err(Im$[\tilde{\mu}_i]$)	-	-	5.4%

TABLE 2. Count of misclassified elements.

	case I	case II	case III
# of misclassified elements	344	549	68
total # of elements	79360	79360	30488

6. CONCLUDING REMARKS

In this work, we have developed a data-driven framework for the identification of spatially-resolved elastic and viscoelastic properties in heterogeneous solids. By leveraging the mixed energy functions of Cherkaev and

Gibiansky [28], we have recast viscoelastic constitutive laws in convex variational form, enabling the use of the duality gap as a natural cost functional for inverse identification. The resulting procedure, combined with DDI initialization, k-planes clustering and principal component analysis, provides a robust methodology that remains effective on several examples of growing complexity.

Beyond offering an alternative to classical parameter-fitting approaches, we demonstrate the utility of data-driven methods for uncovering spatially heterogeneous material properties from full-field experimental measurements. Taken together, these results suggest a pathway toward more comprehensive frameworks for material characterization, where empirical data, convex variational principles, and data-driven inference jointly enable robust identification of heterogeneous materials at high resolution.

Nevertheless, several open challenges remain. The identifiability of complex moduli in general settings, convergence with respect to measurement resolution, and the extension to nonlinear and rate-dependent constitutive behaviors all require further study. In particular, an important open direction is the identification of heterogeneous material parameters in nonlinear (visco)elasticity, a problem that remains highly challenging even under assumptions ensuring well-posedness of the forward problem [8]. In parallel, integrating our framework with emerging high-throughput material characterization approaches offers a promising avenue for enhancing both accuracy and scalability.

Several enhancements and extensions can already be envisioned, such as including multiaxial material response, combining images obtained from different loading cases (boundary conditions, frequency). Adapting the clustering strategy to consider different frequencies, with varying moduli but constant morphology, should for example reinforce identifiability.

As discussed in the introduction, the final objective is of course to work from real field measures, obtained by ultrasound echography or magnetic resonance imaging for example. The challenges will then be linked to the available resolution of images, which may be compensated by combining several images in the identification process.

Acknowledgements

MO gratefully acknowledges the financial support of the Centre Internacional de Métodes Numerics en Enginyeria (CIMNE), Universitat Politècnica de Catalunya, Spain, under the auspices of the UNESCO Chair for Numerical Methods in Engineering. LS gratefully acknowledge the financial support of Nantes Université excellence program NExT, through the funding of International Research Partnership project iDDrEAM.

References

[1] H. Bui, Introduction aux problèmes inverses en mécanique des matériaux, Collection de la Direction des Etudes et Recherches d'Electricité de France, Eds Eyrolles, 1993.

[2] M. Sutton, J.-J. Orteu, H. Schreier, Image Correlation for Shape, Motion and Deformation Measurements. Basic Concepts, Theory and Applications, Springer, 2009.
[3] A. Buljac, C. Jailin, A. Mendoza, J. Neggers, T. Taillandier-Thomas, A. Bouterf, B. Smaniotto, F. Hild, S. Roux, Digital volume correlation: Review of progress and challenges, Experimental Mechanics 58 (2018) 661–708.
[4] X. Li, C. C. Roth, D. Mohr, Machine-learning based temperature- and rate-dependent plasticity model: Application to analysis of fracture experiments on dp steel, International Journal of Plasticity 118 (2019) 320–344.
[5] H. Jin, T. Jiao, R. J. Clifton, K.-S. Kim, Dynamic fracture of a bicontinuously nanostructured copolymer: A deep-learning analysis of big-data-generating experiment, Journal of the Mechanics and Physics of Solids 164 (2022) 104898.
[6] L. V. Hiscox, C. L. Johnson, E. Barnhill, M. D. McGarry, J. Huston, E. J. Van Beek, J. M. Starr, N. Roberts, Magnetic resonance elastography (mre) of the human brain: technique, findings and clinical applications, Physics in Medicine & Biology 61 (24) (2016) R401.
[7] L. V. Hiscox, H. Schwarb, M. D. McGarry, C. L. Johnson, Aging brain mechanics: Progress and promise of magnetic resonance elastography, Neuroimage 232 (2021) 117889.
[8] S. Conti, M. Ortiz, A well-posed variational approach to the identification and convergent approximation of material laws from boundary data, ZAMM-Journal of Applied Mathematics and Mechanics/Zeitschrift für Angewandte Mathematik und Mechanik 105 (7) (2025) e70132.
[9] J. Martins, A. Andrade-Campos, S. Thuillier, Comparison of inverse identification strategies for constitutive mechanical models using full-field measurements, International Journal of Mechanical Sciences 145 (2018) 330–345.
[10] C. Fefferman, S. Mitter, H. Narayanan, Testing the manifold hypothesis, Journal of the American Mathematical Society 29 (4) (2016) 983–1049.
[11] H. N. Nguyen, L. Chamoin, C. H. Minh, mcre-based parameter identification from full-field measurements: Consistent framework, integrated version, and extension to nonlinear material behaviors, Computer Methods in Applied Mechanics and Engineering 400 (2022) 115461.
[12] J. C. Brigham, W. Aquino, Inverse viscoelastic material characterization using pod reduced-order modeling in acoustic–structure interaction, Computer Methods in Applied Mechanics and Engineering 198 (9-12) (2009) 893–903.
[13] A. A. Oberai, N. H. Gokhale, G. R. Feijóo, Solution of inverse problems in elasticity imaging using the adjoint method, Inverse problems 19 (2) (2003) 297.
[14] M. Bonnet, A. Constantinescu, Inverse problems in elasticity, Inverse problems 21 (2) (2005) R1.
[15] B. Ni, H. Gao, A deep learning approach to the inverse problem of modulus identification in elasticity, Mrs Bulletin 46 (2021) 19–25.
[16] E. Zhang, M. Yin, G. E. Karniadakis, Physics-informed neural networks for nonhomogeneous material identification in elasticity imaging, arXiv preprint arXiv:2009.04525 (2020).
[17] A. Leygue, M. Coret, J. Réthoré, L. Stainier, E. Verron, Data-based derivation of material response, Computer Methods in Applied Mechanics and Engineering 331 (2018) 184–196.
[18] S. Avril, M. Bonnet, A.-S. Bretelle, M. Grédiac, F. Hild, P. Ienny, F. Latourte, D. Lemosse, S. Pagano, E. Pagnacco, F. Pierron, Overview of identification methods of mechanical parameters based on full-field measurements, Experimental Mechanics 48 (2008) 381–402.
[19] M. Flaschel, S. Kumar, L. De Lorenzis, Unsupervised discovery of interpretable hyperelastic constitutive laws, Computer Methods in Applied Mechanics and Engineering 381 (2021) 113852.

[20] M. Dalémat, M. Coret, A. Leygue, E. Verron, Measuring stress field without constitutive equation, Mechanics of Materials 136 (2019) 103087.
[21] L. Costecalde, A. Leygue, M. Coret, E. Verron, Data-driven identification of hyperelastic models by measuring the strain energy density field, Rubber Chemistry and Technology 96 (4) (2023) 443–454.
[22] R. Langlois, M. Coret, J. Réthoré, Non-parametric stress field estimation for history-dependent materials: Application to ductile material exhibiting piobert–lüders localization bands, Strain 58 (4) (2022).
[23] A. Vinel, R. Seghir, J. Berthe, G. Portemont, J. Réthoré, Experimental characterization of material strain-rate dependence based on full-field data-driven identification, International Journal of Impact Engineering 194 (2024) 105083.
[24] G. Valdés-Alonzo, C. Binetruy, B. Eck, A. García-González, A. Leygue, Phase distribution and properties identification of heterogeneous materials: A data-driven approach, Computer Methods in Applied Mechanics and Engineering 390 (2022) 114354.
[25] E. Herbert, W. Oliver, G. Pharr, Nanoindentation and the dynamic characterization of viscoelastic solids, Journal of physics D: applied physics 41 (7) (2008) 074021.
[26] M. Gao, J. H. Perepezko, Mapping the viscoelastic heterogeneity at the nanoscale in metallic glasses by static force spectroscopy, Nano Letters 20 (10) (2020) 7558–7565.
[27] C. Franck, S. A. Maskarinec, D. A. Tirrell, G. Ravichandran, Three-dimensional traction force microscopy: a new tool for quantifying cell-matrix interactions, PloS one 6 (3) (2011) e17833.
[28] A. V. Cherkaev, L. V. Gibiansky, Variational principles for complex conductivity, viscoelasticity, and similar problems in media with complex moduli, Journal of Mathematical Physics 35 (1) (1994) 127–145. doi:10.1063/1.530782.
[29] A. Ben-Tal, G. Eiger, V. Gershovitz, Global minimization by reducing the duality gap, Mathematical programming 63 (1) (1994) 193–212.
[30] B. Banerjee, T. F. Walsh, W. Aquino, M. Bonnet, Large scale parameter estimation problems in frequency-domain elastodynamics using an error in constitutive equation functional, Computer methods in applied mechanics and engineering 253 (2013) 60–72.
[31] K. Weinberg, L. Stainier, S. Conti, M. Ortiz, Data-driven games in computational mechanics, Computer Methods in Applied Mechanics and Engineering 417 (2023) 116399.
[32] M. Bonnet, P. Salasiya, B. B. Guzina, Modified error-in-constitutive-relation (mecr) framework for the characterization of linear viscoelastic solids, Journal of the Mechanics and Physics of Solids (2024) 105746.
[33] M. I. Diaz, W. Aquino, M. Bonnet, A modified error in constitutive equation approach for frequency-domain viscoelasticity imaging using interior data, Computer methods in applied mechanics and engineering 296 (2015) 129–149.
[34] R. Rockafellar, Convex Analysis, Princeton Landmarks in Mathematics and Physics, Princeton University Press, 1997.
[35] P. S. Bradley, O. L. Mangasarian, K-plane clustering, Journal of Global optimization 16 (2000) 23–32.
[36] M. C. Tsakiris, R. Vidal, Hyperplane clustering via dual principal component pursuit, in: International conference on machine learning, PMLR, 2017, pp. 3472–3481.
[37] M. Ortiz, Linear viscoelasticity: Mechanics, analysis and approximation, arXiv preprint arXiv:2509.03485 (2025).
[38] A. Wineman, Nonlinear viscoelastic solids—a review, Mathematics and mechanics of solids 14 (3) (2009) 300–366.
[39] R. Schapery, Nonlinear viscoelastic solids, International journal of solids and structures 37 (1-2) (2000) 359–366.

[40] W. G. Knauss, I. Emri, Non-linear viscoelasticity based on free volume consideration, in: computational methods in nonlinear structural and solid mechanics, Elsevier, 1981, pp. 123–128.
[41] W. Wirtinger, Zur formalen theorie der funktionen von mehr komplexen veränderlichen, Mathematische Annalen 97 (1) (1927) 357–375. doi:10.1007/BF01447872.
[42] T. Kirchdoerfer, M. Ortiz, Data-driven computational mechanics, Computer Methods in Applied Mechanics and Engineering 304 (2016) 81–101.
[43] H. Salahshoor, M. Ortiz, Model-free data-driven viscoelasticity in the frequency domain, Computer Methods in Applied Mechanics and Engineering 403 (2023) 115657.
[44] R. Eggersmann, L. Stainier, M. Ortiz, S. Reese, Efficient data structures for model-free data-driven computational mechanics, Computer Methods in Applied Mechanics and Engineering 382 (2021) 113855. doi:10.1016/j.cma.2021.113855.
[45] S. Conti, S. Müller, M. Ortiz, Data-driven problems in elasticity, Archive for Rational Mechanics and Analysis 229 (1) (2018) 79–123.
[46] A. Leygue, On the formulation and convergence of Data-Driven Identification, Comptes Rendus. Mécanique 353 (2025) 761–773.
[47] N. Hachem, A. Leygue, L. Stainier, Mathematical and numerical assessment of data-driven identification method applied to nonlinear elasticity, Computer Methods in Applied Mechanics and Engineering 446 (2025) 118273.
[48] G. Valdés-Alonzo, Identification of material properties and phase distribution of heterogeneous materials through data-driven computational methods : Towards an enhaced constitutive space, Ph.D. thesis, École centrale de Nantes ; Universitat politècnica de Catalunya - BarcelonaTech (2022).
URL `https://theses.hal.science/tel-04056941`
[49] P. Bayly, P. Massouros, E. Christoforou, A. Sabet, G. Genin, Magnetic resonance measurement of transient shear wave propagation in a viscoelastic gel cylinder, Journal of the Mechanics and Physics of Solids 56 (5) (2008) 2036–2049.
[50] R. J. Okamoto, E. H. Clayton, P. V. Bayly, Viscoelastic properties of soft gels: comparison of magnetic resonance elastography and dynamic shear testing in the shear wave regime, Physics in Medicine & Biology 56 (19) (2011) 6379.
[51] J. Bercoff, S. Chaffai, M. Tanter, L. Sandrin, S. Catheline, M. Fink, J. Gennisson, M. Meunier, In vivo breast tumor detection using transient elastography, Ultrasound in medicine & biology 29 (10) (2003) 1387–1396.
[52] L. Pallwein, M. Mitterberger, P. Struve, G. Pinggera, W. Horninger, G. Bartsch, F. Aigner, A. Lorenz, F. Pedross, F. Frauscher, Real-time elastography for detecting prostate cancer: preliminary experience, BJU international 100 (1) (2007) 42–46.
[53] P. Virtanen, R. Gommers, T. E. Oliphant, M. Haberland, T. Reddy, D. Cournapeau, E. Burovski, P. Peterson, W. Weckesser, J. Bright, S. J. van der Walt, M. Brett, J. Wilson, K. J. Millman, N. Mayorov, A. R. J. Nelson, E. Jones, R. Kern, E. Larson, C. J. Carey, İ. Polat, Y. Feng, E. W. Moore, J. VanderPlas, D. Laxalde, J. Perktold, R. Cimrman, I. Henriksen, E. A. Quintero, C. R. Harris, A. M. Archibald, A. H. Ribeiro, F. Pedregosa, P. van Mulbregt, SciPy 1.0 Contributors, SciPy 1.0: Fundamental Algorithms for Scientific Computing in Python, Nature Methods 17 (2020) 261–272. doi:10.1038/s41592-019-0686-2.
[54] F. Pedregosa, G. Varoquaux, A. Gramfort, V. Michel, B. Thirion, O. Grisel, M. Blondel, P. Prettenhofer, R. Weiss, V. Dubourg, J. Vanderplas, A. Passos, D. Cournapeau, M. Brucher, M. Perrot, E. Duchesnay, Scikit-learn: Machine learning in Python, Journal of Machine Learning Research 12 (2011) 2825–2830.

[1]Department of Civil and Environmental Engineering, Duke University, 101 Science Dr. Durham, NC 27708. [2]Department of Mechanical Engineering and Materials Science, Duke University, 101 Science Dr. Durham, NC 27708. [3]Division of Engineering and Applied Science, California Institute of Technology, 1200 E. California Blvd., Pasadena, CA 91125. [4]Centre Internacional de Métodes Numerics en Enginyeria (CIMNE), Universitat Politècnica de Catalunya, Jordi Girona 1, 08034 Barcelona, Spain. [5]Nantes Université, École Centrale Nantes, CNRS, GeM, UMR6183, 1 rue de la Noë, Nantes, F-44300, France.,

Email address: laurent.stainier@ec-nantes.fr